J|A|C|S ARTICLES

Published on Web 07/24/2009

Understanding Structure−Mobility Relations for Perylene Tetracarboxydiimide Derivatives

Valentina Marcon,*,† Dag W. Breiby,‡ Wojciech Pisula,†,⊥ Julie Dahl,‡ James Kirkpatrick,§ Sameer Patwardhan,|| Ferdinand Grozema,|| and Denis Andrienko*,†

Max Planck Institute for Polymer Research, Ackermannweg 10, 55128 Mainz, Germany, Department of Physics, Norwegian University of Science and Technology, Høgskoleringen 5, N-7491 Trondheim, Norway, Department of Physics, Imperial College London, Prince Consort Road, London SW7 2BW, United Kingdom, and DelftChemTech, Delft University of Technology, Julianalaan 136, 2628 BL Delft, The Netherlands

Received February 13, 2009; E-mail: marcon@mpip-mainz.mpg.de; denis.andrienko@mpip-mainz.mpg.de

Abstract: Discotic mesophases are known for their ability to self-assemble into columnar structures and can serve as semiconducting molecular wires. Charge carrier mobility along these wires strongly depends on molecular packing, which is controlled by intermolecular interactions. By combining wide-angle X-ray scattering experiments with molecular dynamics simulations, we elucidate packing motifs of a perylene tetracarboxdiimide derivative, a task which is hard to achieve by using a single experimental or theoretical technique. We then relate the charge mobility to the molecular arrangement, both by pulse-radiolysis time-resolved microwave conductivity experiments and simulations based on the non-adiabatic Marcus charge transfer theory. Our results indicate that the helical molecular arrangement with the 45° twist angle between the neighboring molecules favors hole transport in a compound normally considered as an n-type semiconductor. Statistical analysis shows that the transport is strongly suppressed by structural defects. By linking molecular packing and mobility, we eventually provide a pathway to the rational design of perylenediimide derivatives with high charge mobilities.

I. Introduction

A quintessential property of flat aromatic molecules furnished with flexible side chains is their ability to self-organize into columnar structures, with conjugated molecular cores stacked on top of each other and linear or branched side chains surrounding the columns. Appropriate molecular arrangement allows for one-dimensional transport of charge carriers along the columns, due to the overlap of the π-orbitals of the neighboring molecules in a column, rendering these materials as organic semiconductors. Indeed, discotics have already been found suitable for applications in organic field-effect transistors and solar cells.[1−5]

A key property of discotics is that high charge carrier mobilities, up to 1 $cm^2\ V^{-1}\ s^{-1}$, can be achieved by either optimizing the electronic structure of compounds, decreasing reorganization energies and increasing electronic wave function couplings,[6,7] or systematically varying the substituents and processing to achieve ordered and defect-free molecular arrangements.[7−9]

A practical route to improve mobility includes synthesis, optimization of processing conditions, characterization of morphology, and measurements of the mobility of a new material.[7,10−14] Repeating this procedure for a set of compounds,

† Max Planck Institute for Polymer Research.
‡ Norwegian University of Science and Technology.
§ Imperial College London.
|| Delft University of Technology.
⊥ Present address: Evonik Degussa GmbH, Process Technology and Engineering, Process Technology - New Processes, Rodenbacher Chaussee 4, 63457 Hanau-Wolfgang, Germany.

(1) Adam, D.; Schuhmacher, P.; Simmerer, J.; Haussling, L.; Siemensmeyer, K.; Etzbach, K. H.; Ringsdorf, H.; Haarer, D. *Nature* **1994**, *371* (6493), 141–143.
(2) Schmidt-Mende, L.; Fechtenkotter, A.; Müllen, K.; Moons, E.; Friend, R.; MacKenzie, J. *Science* **2001**, *293* (5532), 1119–1122.
(3) Hoeben, F.; Jonkheijm, P.; Meijer, E.; Schenning, A. *Chem. Rev.* **2005**, *105* (4), 1491–1546.
(4) Sergeyev, S.; Pisula, W.; Geerts, Y. H. *Chem. Soc. Rev.* **2007**, *36* (12), 1902–1929.
(5) Wu, J.; Pisula, W.; Müllen, K. *Chem. Rev.* **2007**, *107* (3), 718–747.
(6) Lemaur, V.; Da Silva Filho, D.; Coropceanu, V.; Lehmann, M.; Geerts, Y.; Piris, J.; Debije, M.; Van de Craats, A.; Senthilkumar, K.; Siebbeles, L.; Warman, J.; Bredas, J.; Cornil, J. *J. Am. Chem. Soc.* **2004**, *126*, 3271–3279.
(7) Feng, X.; Marcon, V.; Pisula, W.; Kirkpatrick, J.; Grozema, F.; Andrienko, D.; Kremer, K.; Müllen, K. *Nat. Mater.* **2009**, *8*, 421–426.
(8) Feng, X.; Pisula, W.; Müllen, K. *J. Am. Chem. Soc.* **2007**, *129* (46), 14116–14117.
(9) Feng, X. L.; Wu, J. S.; Ai, M.; Pisula, W.; Zhi, L. J.; Rabe, J. P.; Müllen, K. *Ang. Chem., Int. Ed.* **2007**, *46* (17), 3033–3036.
(10) van de Craats, A. M.; Warman, J. M.; Fechtenkötter, A.; Brand, J. D.; Harbison, M. A.; Müllen, K. *Adv. Mater.* **1999**, *11*, 1469–1472.
(11) Fechtenkötter, A.; Saalwaechter, K.; Harbison, M. A.; Müllen, K.; Spiess, H. W. *Angew. Chem., Int. Ed.* **1999**, *38*, 3039–3042.
(12) Debije, M. G.; Piris, J.; de Haas, M. P.; Warman, J. M.; Tomovic, Z.; Simpson, C. D.; Watson, M. D.; Müllen, K. *J. Am. Chem. Soc.* **2004**, *126* (14), 4641–4645.
(13) Kastler, M.; Pisula, W.; Laquai, F.; Kumar, A.; Davies, R. J.; Baluschev, S.; Garcia-Gutierrez, M. C.; Wasserfallen, D.; Butt, H. J.; Riekel, C.; Wegner, G.; Müllen, K. *Adv. Mater.* **2006**, *18* (17), 2255.
(14) Pisula, W.; Kastler, M.; Wasserfallen, D.; Mondeshki, M.; Piris, J.; Schnell, I.; Müllen, K. *Chem. Mater.* **2006**, *18* (16), 3634–3640.

 10.1021/ja900963v CCC: $40.75

one should be able to formulate a set of empirical rules, or structure-processing-property relationships, and proceed further with the *rational* design of these compounds. The weak link in this scheme is that it is practically impossible to disentangle whether the improvement comes from a better electronic structure or a superior morphology, because both are affected by the change in the chemical structure. In particular, it is difficult to characterize the (partially disordered) material morphology with a high level of detail. Wide-angle X-ray scattering (WAXS) in transmission geometry and solid-state nuclear magnetic resonance (NMR) are routinely employed and somewhat complement each other.

WAXS provides information about periodically repeated structures over distances that are large compared to the molecular entities, i.e., molecular packing motifs, including orientation distribution functions.[14−16] Being a complementary technique, solid-state NMR can shed some light on the local molecular packing.[14,17−19] Both methods, however, provide only *averages* over the molecular ensemble and, as such, do not contain full information about the *distributions* of molecular positions and orientations.

At the same time, charge dynamics of partially ordered semiconductors is sensitive to the molecular arrangement on all length scales.[20,21] Indeed, transfer integrals and charge hopping rates strongly depend on the chemical composition and *local* molecular ordering while the global charge carrier pathway is determined by the *large scale* morphology and presence of defects.

In this situation, modeling becomes a necessity: it assists in identifying correct molecular packing motifs,[7,22−24] quantifies the degree of local disorder, and links both of these to the charge carrier mobility.[7,20,21,25−29] In our previous work we have established a link between charge mobility and morphology for the derivatives of hexabenzocoronene[21,23] and designed a new class of triangularly shaped discotics[7] with high charge carrier mobility. In this paper we attempt to establish the structure−mobility relations for the heptyloctyl substituted perylene tetracarboxydiimide derivative, PDI-$C_{8,7}$. The chemical structure of PDI-$C_{8,7}$ is shown in Figure 1a.

Various perylenediimide (PDI) derivatives have found application in different areas of organic electronics, such as all-organic photovoltaic solar cells[2,30,31] and field-effect transistors.[32,33] Compounds based on PDI are some of the best and most used n-type semiconductors,[32,34] though their electron and hole mobilities are rather similar.[35] Mobilities up to 0.6 $cm^2\ V^{-1}\ s^{-1}$ have been reported for thin PDI films.[36,37] PDI derivatives can self-assemble in structures with different packing motifs,[38] which also results in different charge mobilities.[39] Their self-organizing abilities can be controlled by introducing hydrogen bonding,[40] metal-ion coordination,[41] or by changing the geometry of the side groups.[42,43]

The paper is organized as follows. We first describe a model of supramolecular helical arrangement based on WAXS experiments. Further support is given to this model by calculating WAXS patterns from molecular dynamics (MD) snapshots. The obtained MD morphologies, in combination with the high-temperature non-adiabatic Marcus expression for charge transfer rates and kinetic Monte Carlo simulations of charge carrier dynamics, are used to predict charge mobility in the system which is then compared to pulse-radiolysis time-resolved microwave conductivity (PR-TRMC) measurements. Finally, we identify the ideal packing structure for charge transport of PDI derivatives.

II. Molecular Arrangement from WAXS Experiments and Molecular Dynamics Simulations

For the structural investigations of the crystalline phase, WAXS experiments on extruded filaments of diameter 0.7 mm were performed;[44] see Supporting Information for full details. The WAXS pattern of the crystalline phase of PDI-$C_{8,7}$ is shown in Figure 2a. As evidenced by the sharp Bragg peaks, PDI-$C_{8,7}$ has a high degree of crystallinity, and the differential scanning calorimetry revealed only one phase transition at 130 °C from the crystalline to the isotropic phase. The wide arcs imply that

(15) Breiby, D. W.; Bunk, O.; Pisula, W.; Solling, T. I.; Tracz, A.; Pakula, T.; Müllen, K.; Nielsen, M. M. *J. Am. Chem. Soc.* **2005**, *127* (32), 11288–11293.
(16) Breiby, D.; Hansteen, F.; Pisula, W.; Bunk, O.; Kolb, U.; Andreasen, J.; Mullen, K.; Nielsen, M. *J. Phys. Chem. B* **2005**, *109* (42), 22319–22325.
(17) Ochsenfeld, C. *Phys. Chem. Chem. Phys.* **2000**, *2* (10), 2153–2159.
(18) Ochsenfeld, C.; Brown, S. P.; Schnell, I.; Gauss, J.; Spiess, H. W. *J. Am. Chem. Soc.* **2001**, *123* (11), 2597–2606.
(19) Hansen, M. R.; Graf, R.; Sebastiani, D. *J. Am. Chem. Soc.* **2009**, *131* (14), 5251–5256.
(20) Kirkpatrick, J.; Marcon, V.; Nelson, J.; Kremer, K.; Andrienko, D. *Phys. Rev. Lett.* **2007**, *98*, 227402.
(21) Kirkpatrick, J.; Marcon, V.; Kremer, K.; Nelson, J.; Andrienko, D. *J. Chem. Phys.* **2008**, *129*, 094506.
(22) Cinacchi, G.; Colle, R.; Tani, A. *J. Phys. Chem. B* **2004**, *108* (23), 7969–7977.
(23) Marcon, V.; Vehoff, T.; Kirkpatrick, J.; Jeong, C.; Yoon, D. Y.; Kremer, K.; Andrienko, D. *J. Chem. Phys.* **2008**, *129*, 094505.
(24) Marcon, V.; Kirkpatrick, J.; Pisula, W.; Andrienko, D. *Phys. Status Solidi B* **2008**, *245*, 820–824.
(25) Kirkpatrick, J.; Marcon, V.; Nelson, J.; Andrienko, D. *Phys. Status Solidi B* **2008**, *245*, 835–838.
(26) Kwiatkowski, J. J.; Nelson, J.; Li, H.; Bredas, J. L.; Wenzel, W.; Lennartz, C. *Phys. Chem. Chem. Phys.* **2008**, *10*, 1852–1858.
(27) Nagata, Y.; Lennartz, C. *J. Chem. Phys.* **2008**, *129* (3), 034709.
(28) Cheung, D. L.; Troisi, A. *Phys. Chem. Chem. Phys.* **2008**, *10* (39), 5941–5952.
(29) Troisi, A.; Cheung, D. L.; Andrienko, D. *Phys. Rev. Lett.* **2009**, *102*, 116602.
(30) Halls, J.; Friend, R. *Synth. Met.* **1997**, *85*, 1307–1308.
(31) Im, C.; Tian, W.; Bassler, H.; Fechtenkotter, A.; Watson, M.; Müllen, K. *Synth. Met.* **2003**, *139* (3), 683–686.
(32) Horowitz, G.; Kouki, F.; Spearman, P.; Fichou, D.; Nogues, C.; Pan, X.; Garnier, F. *Adv. Mater.* **1996**, *8* (3), 242.
(33) Jones, B.; Ahrens, M.; Yoon, M.; Facchetti, A.; Marks, T.; Wasielewski, M. *Ang. Chem., Int. Ed.* **2004**, *43* (46), 6363–6366.
(34) Chesterfield, R.; McKeen, J.; Newman, C.; Ewbank, P.; da Silva, D.; Bredas, J.; Miller, L.; Mann, K.; Frisbie, C. *J. Phys. Chem. B* **2004**, *108* (50), 19281–19292.
(35) Kim, J.; Chung, I.; Kim, Y.; Yu, J. *Chem. Phys. Lett.* **2004**, *398*, 367–371.
(36) Struijk, C.; Sieval, A.; Dakhorst, J.; van Dijk, M.; Kimkes, P.; Koehorst, R.; Donker, H.; Schaafsma, T.; Picken, S.; van de Craats, A.; Warman, J.; Zuilhof, H.; Sudholter, E. *J. Am. Chem. Soc.* **2000**, *122* (45), 11057–11066.
(37) Malenfant, P.; Dimitrakopoulos, C.; Gelorme, J.; Kosbar, L.; Graham, T.; Curioni, A.; Andreoni, W. *App. Phys. Lett.* **2002**, *80* (14), 2517–2519.
(38) Nolde, F.; Pisula, W.; Müller, S.; Kohl, C.; Müllen, K. *Chem. Mater.* **2006**, *18*, 3715.
(39) Chen, Z. J.; Stepanenko, V.; Dehm, V.; Prins, P.; Siebbeles, L. D. A.; Seibt, J.; Marquetand, P.; Engel, V.; Wurthner, F. *Chem.—Eur. J.* **2007**, *13* (2), 436–449.
(40) Zhang, X.; Chen, Z.; Wurthner, F. *J. Am. Chem. Soc.* **2007**, *129* (16), 4886.
(41) Wurthner, F. *Chem. Commun.* **2004**, (14), 1564–1579.
(42) van de Craats, A.; Warman, J.; Schlichting, P.; Rohr, U.; Geerts, Y.; Müllen, K. *Synth. Met.* **1999**, *102*, 1550–1551.
(43) Chen, Z.; Stepanenko, V.; Dehm, V.; Prins, P.; Siebbeles, L. D. A.; Seibt, J.; Marquetand, P.; Engel, V.; Würthner, F. *Chem.—Eur. J.* **2007**, *13*, 436.
(44) Pisula, W.; Tomovic, Z.; Simpson, C.; Kastler, M.; Pakula, T.; Müllen, K. *Chem. Mater.* **2005**, *17*, 4296.

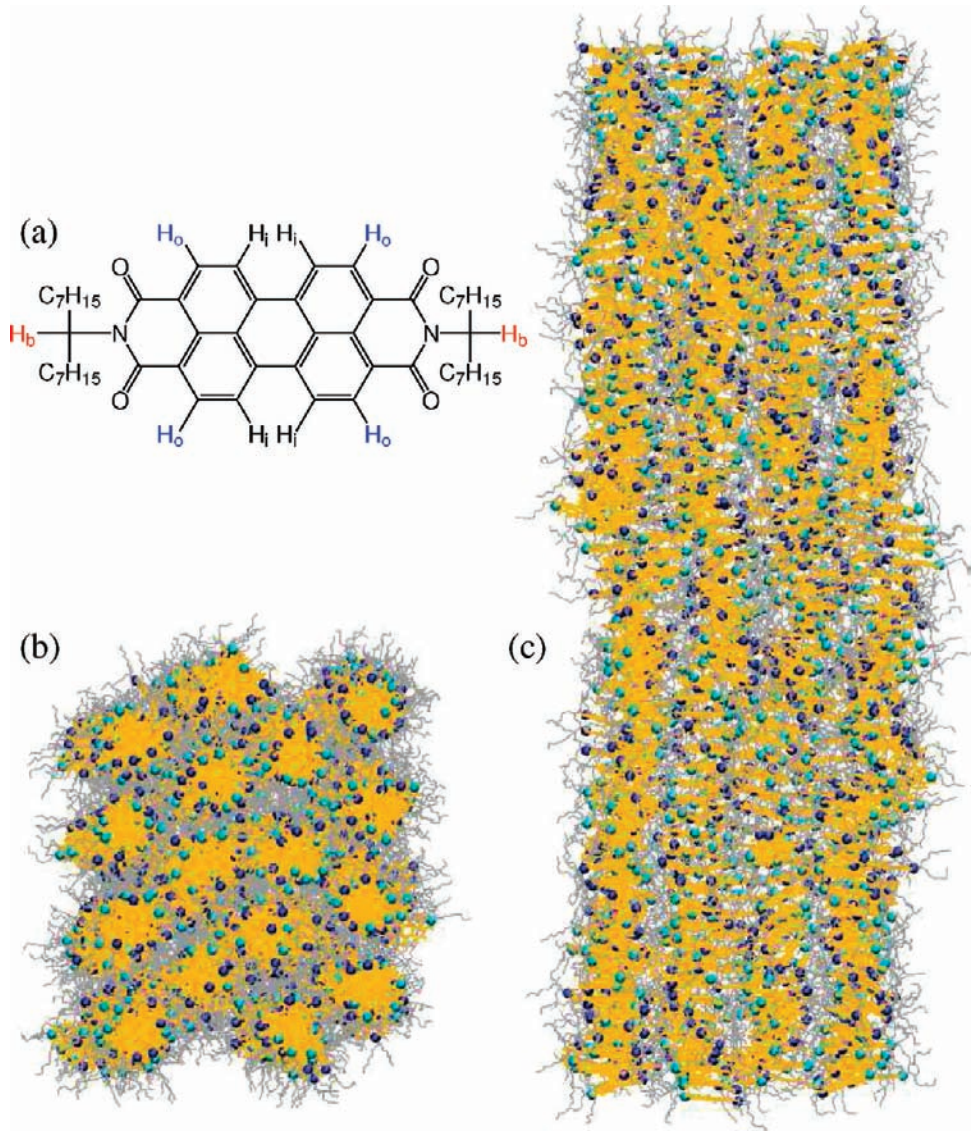

Figure 1. (a) Chemical structure of PDI-$C_{8,7}$ derivative, the labeling of hydrogen atoms is explained in Section III. (b) Top and (c) side views of a molecular dynamics snapshot of a hexagonal columnar arrangement; 960 molecules are stacked in columns of 60 molecules each. $T = 400$ K. The side view clearly shows undulations and defects in the columnar arrangement. The carbon atoms of the conjugated core are shown in yellow, the two nitrogens are in dark and light blue, and the side chains are in gray.

the material can be considered a textured powder, exhibiting fiber symmetry about an axis coinciding with the extrusion direction of the filament. There are reflections both along the equator and meridian of the 2D pattern, and importantly, there are also scattering features that have maxima outside these lines. We shall show that columnar structures[45,46] are a consistent and likely interpretation of the data.

The positions of the distinct *equatorial* reflections can be fitted by a monoclinic unit cell with $a = 21.9$ Å, $b = 17.9$ Å, $c = 3.55$ Å, and $\gamma = 97.8°$ (see Figures 2b,c and Supporting Information). Throughout, we describe the scattering in terms of the scattering vector Q, whose magnitude can be associated with distances in real space by $Q = 2\pi/\lambda$. The main *meridional* reflection is related to the π-stacking period of 3.55 Å, which is taken as the c-parameter of the unit cell. Thereby the molecular cores arrange with their disk plane normals parallel to the columnar axis. Some of the intermediate-Q diffraction rings exhibit intensity maxima located off the equator. This can be interpreted as evidence for a regular intracolumnar packing. The meridional reflection at the smallest scattering angle is attributed to a spacing of 12.6 Å. Taking into account the π-stacking distance of 3.55 Å ($Q = 1.77$ Å^{-1}), it can be assumed that the band of higher intensity at a $Q \approx 0.44 \pm 0.03$ Å^{-1} on the meridian represents correlations with a periodicity of roughly four times the neighboring distance along the columnar stack. This suggests a helical molecular arrangement within the columns, with a ~45° rotation angle between neighboring molecules. The observations corroborate the previously reported packing motifs of perylene derivatives, which were also interpreted as displaying helical stacks of the discotic molecules.[43,47]

(45) Laschat, S.; Baro, A.; Steinke, N.; Giesselmann, F.; Hägele, C.; Scalia, G.; Judele, R.; Kapatsina, E.; Sauer, S.; Schreivogel, A.; Tosoni, M. *Angew. Chem., Int. Ed.* **2007**, *119*.
(46) Sergeyev, S.; Pisula, W.; Geerts, Y. H. *Chem. Soc. Rev.* **2007**, *36*, 1902–1929.
(47) Dehm, V.; Chen, Z.; Baumeister, U.; Prins, P.; Siebbeles, L. D. A.; Würthner, F. *Org. Lett.* **2007**, *9*, 1085–1088.

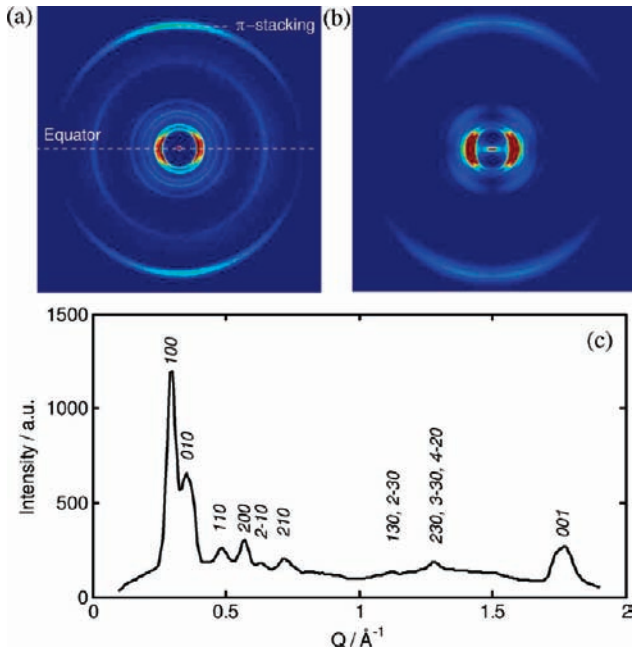

Figure 2. (a) Experimental WAXS pattern of an extruded filament of heptyloctyl substituted PDI in a crystalline phase. (b) WAXS pattern generated from the molecular dynamics snapshots, showing good agreement with the experimental pattern. (c) Radial integration of the experimental 2D pattern with the assignment of Miller indices to the reflections.

To strengthen the model hypothesis based on inspecting the experimental WAXS images, we have calculated WAXS patterns using the morphologies obtained from the MD simulations. The MD simulation details are discussed in Section III, and the diffraction pattern calculations are outlined in Supporting Information and refs 48 and 49.

The results are shown in Figure 2b. The MD structures yield pronounced π-stack peaks at $Q \approx 1.75 \pm 0.05$ Å^{-1}. In addition, there are scattering features at small Q-values of 0.2−0.6 Å^{-1}, consistent with the anticipated column widths. The experimental image has two strong equatorial reflections surrounded by three weaker rings in the low-Q region and also a Debye−Scherrer ring at intermediate Q.

Upon comparing the experimental and theoretical diffraction patterns, one notes the agreement in showing a "π-stacking" peak at 1.77 Å^{-1}, two strong and several weaker intercolumnar equatorial peaks at the correct Q-values and, particularly gratifying, the existence of peaks off the equatorial and meridional axes at roughly 1/4 of the (meridional) "π-stacking" distance. The main discrepancies relate to the detailed relative peak intensities and the significant equatorial peak at 1.28 Å^{-1}, which indicates correlations not captured by the MD model. This, however, will only weakly affect the molecular packing within the columns and hence will not influence the one-dimensional charge transport. It is clear that the results shown represent substantial improvement when it comes to more rigorous understanding and modeling of partially ordered molecular materials.

III. Local Molecular Ordering by Molecular Dynamics

The role of molecular dynamics (MD) in this work is twofold. First, it helps to clarify the equilibrium value of the helical pitch, the lattice parameters for the 2D arrangement of columns, and the local molecular ordering within the columns. The obtained MD snapshots can be used to calculate WAXS diffraction patterns and to verify predictions of the model based on WAXS experiments. Second, MD provides realistic morphologies that can be used to simulate charge dynamics, which is very sensitive to the relative positions and orientations of neighboring molecules.[6,20,21,25,50]

The systems consisted of 960 molecules stacked in columns of 60 molecules each. A typical MD snapshot for the hexagonal arrangement of columns is shown in Figure 1. Force-field parameters and simulation details are given in the Supporting Information.

Let us first discuss the symmetry of the two-dimensional lattice formed by the columns. To determine the lattice parameters, we prepared several initial configurations with columns arranged on both orthorhombic and hexagonal lattices, with a helical molecular arrangement in the columns and 45° twist angle between the neighboring molecules. The systems were annealed at 400, 450, and 500 K. Upon annealing, the orientational order parameter slowly decreases, which indicates melting of the crystalline phase. However, the lattice symmetry does not change even after annealing at 500 K. We therefore concluded that the MD simulations are too short for a transition from a hexagonal or orthorhombic to monoclinic lattice to occur, contrary to our previous experience with hexabenzocoronenes,[23,51] where a transition between hexagonal and orthorhombic lattices does occur on a time scale accessible to MD. Hence, for a quantitative comparison of calculated and experimental diffraction patterns we used the unit cell provided by the analysis of WAXS patterns, i.e., the angle $\gamma = 97.8°$ was fixed during the equilibration run. We shall mention that the orientational and spatial distributions between the neighboring molecules in columns were not strongly affected by the lattice symmetry. Taking into account that the charge transport is effectively one-dimensional and occurs along the columns, this observation justified our predictions of charge mobility based on the MD snapshots.

To obtain the equilibrium value of the helical pitch, we have prepared starting configurations with four twist angles between the neighboring molecules, 30°, 36°, 45°, 60°, and 90°, which corresponds to 6, 5, 4, 3, and 2 molecules per period. The systems were then annealed for 40 ns at 300 and 400 K. The dependence of the average twist angle between neighboring molecules versus equilibration time (see Supporting Information) shows that the molecular orientation within the columns slowly converges to a helical structure with a ~45° twist angle and the final value of the pitch does not depend on the starting configuration. The computed average value of 47° is in excellent agreement with the WAXS considerations. Convergence is much faster at 400 K, where the equilibrium distribution is reached already after 40 ns. The histograms of the twist angle between neighboring molecules (probability to find two neighbors rotated with respect to each other at an angle ϕ) are shown in Figure 3 illustrating orientational molecular distribution within the columns.

(48) Breiby, D. W.; Lemke, H. T.; Hammershoj, P.; Andreasen, J. W.; Nielsen, M. M. *J. Phys. Chem. C* **2008**, *112*, 4569–4572.
(49) Breiby, D. W.; Bunk, O.; Andreasen, J. W.; Lemke, H. T.; Nielsen, M. M. *J. Appl. Crystallogr.* **2008**, *41*, 262–271.
(50) Andrienko, D.; Kirkpatrick, J.; Marcon, V.; Nelson, J.; Kremer, K. *Phys. Status Solidi B* **2008**, *245*, 830–834.
(51) Andrienko, D.; Marcon, V.; Kremer, K. *J. Chem. Phys.* **2006**, *125*, 124902.

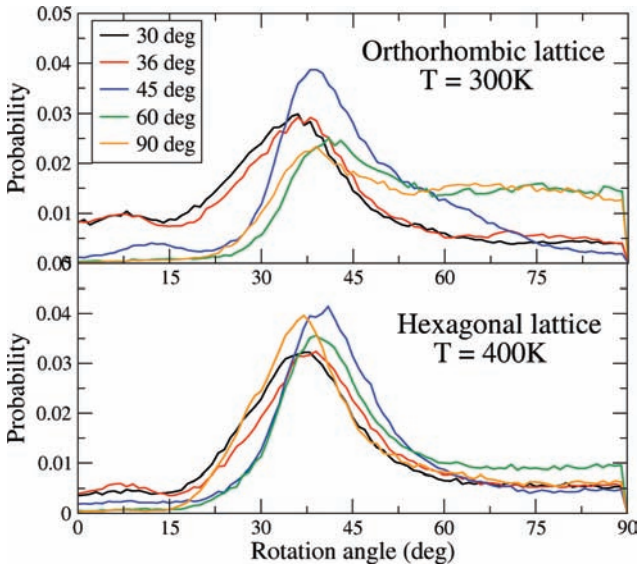

Figure 3. Distribution functions of the twist angle between two neighboring molecules.

Table 1. Dynamic Order Parameters S for the Different Core C−H Moieties of PDI-$C_{8,7}$ Determined from MD Simulations and 2D Rotor-Encoded Solid-State NMR[a]

method	temp (K)	lattice	S (CH_o)	S (CH_i)	S (CH_b)	Q
NMR	300		0.9 ± 0.1	∼1	0.9 ± 0.1	
MD	300	ortho	0.91	0.86	0.96	0.91
	400	hexa	0.86	0.81	0.91	0.87
	400	ortho	0.86	0.81	0.90	0.9
	450	ortho	0.80	0.76	0.83	0.86
	500	ortho	0.62	0.58	0.64	0.65

[a] Experimental data is taken from ref 19. The last column gives the corresponding nematic order parameter Q according to eq 1.

To quantify the degree of molecular ordering, we have calculated the molecular orientational order parameter Q, which is the largest eigenvalue of the order tensor $Q_{\alpha\beta}$:

$$Q_{\alpha\beta} = \left\langle \frac{1}{N}\sum_{i=1}^{N}\left(\frac{3}{2}u_{\alpha}^{(i)}u_{\beta}^{(i)} - \frac{1}{2}\delta_{\alpha\beta}\right)\right\rangle \qquad (1)$$

where $\boldsymbol{u}^{(i)}$ is a unit vector normal to the ith aromatic core, N is the number of the molecules in the system, $\langle\cdots\rangle$ denotes the time average. $Q = 1$ implies perfect alignment of the molecules, with all unit vectors parallel to each other, and $Q = 0$ corresponds to the isotropic angular distribution of the unit vectors. As can be seen from Table 1, the order parameter consistently decreases with temperature as the thermal fluctuations increase the mobility of the side chains. It also does not depend on the lattice symmetry or starting configuration.

It is also instructive to make a link to the recent solid-state NMR results[19] by extracting average interatomic distances and dynamic order parameters from the MD trajectories. The dipolar couplings can be calculated as[52]

$$d_{\mathrm{HH}} = \left\langle \frac{1}{N}\sum_{p=1}^{N}\frac{1}{r_{\mathrm{HH}}^{3}}\right\rangle^{-1/3} \qquad (2)$$

where $\langle\cdots\rangle$ denotes the time average, N is the number of pairs of atoms of interest, and $r_{\mathrm{HH}} = |\boldsymbol{r}_i - \boldsymbol{r}_j|$ is the distance between these atoms, in our case the branching hydrogens H_b of the alkyl chains, as shown in Figure 1a. Note that only the atoms of the neighboring molecules are taken into account.

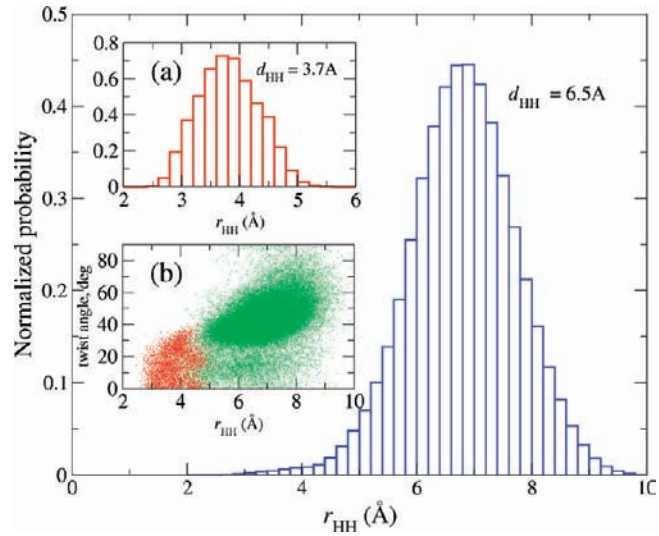

Figure 4. Time-averaged effective intermolecular distance distributions calculated according to eq 2 for pairs of branching hydrogens (H_b) within the molecular stacks of PDI-$C_{8,7}$ molecules. Inset (a) illustrates the same distribution after application of a 5.5 Å dynamic cutoff (see text) and inset (b) displays the correlation between the surviving distances described by the distribution in (a) and the twist angle α between pairs of neighboring PDI-$C_{8,7}$ molecules. Red (green) dots indicate parts of the phase space detected (neglected) by NMR.

The distribution of d_{HH} for branching hydrogens is shown in Figure 4 and provides the average effective intermolecular distance of 6.5 Å, which is much larger than the distance of 3.7 ± 0.1 Å determined experimentally by solid-state NMR.[19] To understand this discrepancy it is important to realize the differences between the two methods. First, MD and NMR are averaging the intermolecular distances on different time scales, μs versus ms, respectively. Second, the NMR experiment uses a double quantum (DQ) filter, where DQ coherences are created (and converted) and also allowed to evolve on a ms time-scale. If two atoms contributing to the signal depart further than ∼5 Å, the dephasing occurs leading to a signal loss. This effect can be incorporated into MD analysis as a dynamical cutoff: pairs of molecules that move during the course of the MD run beyond the cutoff must be neglected. The inset in Figure 4a shows how the initial distribution changes after applying the cutoff of 5.5 Å. This distribution reproduces the effective intermolecular distance of 3.7 ± 0.1 Å determined from NMR.

With the distribution describing the NMR results at hand, it is interesting to investigate what stacking angles these pairs correspond to and thereby gain information about the underlying morphology detected by solid-state NMR. Figure 4b shows the distance versus twist angle correlation. From this plot it can be seen that the NMR experiments in fact only include pairs of neighboring PDI-$C_{8,7}$ molecules with stacking angles smaller than 40°.

Another quantity available from solid-state NMR is the dynamic order parameter, which can be related to the mobility of a moiety of interest. In the MD calculations the dynamic order parameter can be calculated as

(52) Schmidt-Rohr, K.; Spiess, H. W. *Multidimensional Solid-Date NMR and Polymers*; Academic: San Diego, CA 1994.

$$S = \left\langle \frac{1}{N}\sum_{i=1}^{N}\left(\frac{3}{2}(\boldsymbol{M}_i;\boldsymbol{m}_i)^2 - \frac{1}{2}\right)\right\rangle \qquad \boldsymbol{M}_i = \langle \boldsymbol{m}_i \rangle \tag{3}$$

where $\langle \cdots \rangle$ denotes time average, $\boldsymbol{m}_i$ is the vector along the C−H_x group of interest, H_i,H_o,H_b in our particular case; see Figure 1a for the notations.

Calculated dynamical order parameters are summarized in Table 1. At 300 K, where both experimental and calculated data are available, the order parameters show a very good agreement and values $S \approx 1$ are obtained. This indicates that the cores of the PDI-$C_{8,7}$ molecules are quite rigid on both the MD and NMR time scales and also suggests that the PDI-$C_{8,7}$ system is crystalline at 300 K. Moreover, as the temperature is increased the MD results show that PDI-$C_{8,7}$ core becomes more mobile with $S \approx 0.5$.

IV. Charge Mobility: PR-TRMC and Kinetic Monte Carlo Simulations

To obtain charge mobility we have performed the pulse radiolysis time-resolved microwave conductivity measurements,[53] which is described in the Supporting Information. The room temperature mobility $\mu = 0.15 \pm 0.05$ cm^2 V^{-1} s^{-1} is comparable to the mobility observed in the discotic mesophase of hexabenzocoronene[10,54] and semitriangularly shaped polyaromatic hydrocarbons.[7]

To relate microscopic molecular alignment and chemical structure to mobility we used a thermally activated hopping formalism with the rate of hops given by Marcus theory.[6,7,20,21,55] The higher this rate is, the faster the charge carrier (either hole or electron) moves along the column, and the higher the mobility is. The transfer rate depends, in the framework of Marcus theory, on two key parameters: the reorganization energy λ and the transfer integral J.[56]

The reorganization energy λ, which is not dependent on the relative positions/orientations of neighboring molecules, was computed as the sum of the relaxation energies for neutral and positive radicals following ref 6 using B3LYP functional with a triple-ζ split basis set, 6-311 g(d,p), using the GAUSSIAN[57] program. The computed values for the reorganization energies are 0.25 eV for the electrons and 0.14 eV for the holes. The higher the reorganization energy is, the slower the hopping rates are.

The transfer integral J describes the probability of electron tunneling between two neighboring molecules. We compute it within the independent neglect of differential overlap level of theory using a highly optimized ad hoc code that has been shown to give very similar results to density functional theory at a fraction of computational cost.[58] Since the transfer integral is related to the molecular overlap, it is very sensitive to relative orientations and positions of the neighbors. Analyzing the evolution of the transfer integral as a function of the azimuthal rotational angle, which is shown in the inset of Figure 5, we can conclude that the most favorable molecular alignment for hole transport is either a cofacial (0° twist) or 50° twisted one, while for electron transport the best arrangement is either the cofacial one or a 65° twisted one.

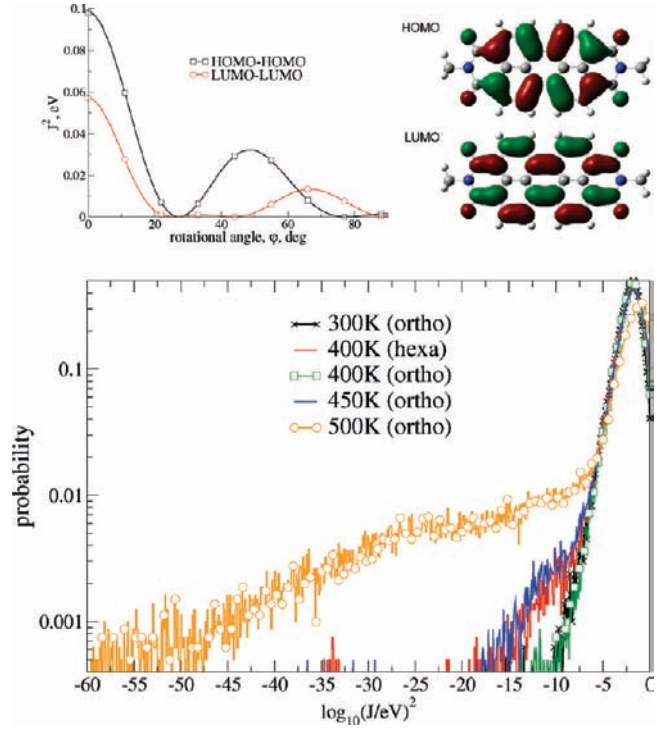

Figure 5. Distribution of the transfer integral between neighboring molecules. Note the logarithmic scale on both axes. Increase of temperature leads to an increase of the orientational and positional disorder manifesting itself in a tail of small J. Since the charge transport is one-dimensional, this tail leads to a significant reduction of the mobility. Inset shows the dependence of the transfer integral J^2, or electronic coupling, on the twist angle between two PDI-$C_{8,7}$ molecules at a distance of 3.5 Å.

Table 2. Simulated and Experimental Mobilities (cm^2 V^{-1} s^{-1})[a]

		lattice, temp			
		ortho, 300 K	hexa, 400 K	ortho, 400 K	ortho, 450,
μ_h	max	0.1	0.1	0.16	0.18
	av	0.06	0.03	0.07	0.04
μ_e	max	0.01	0.01	0.01	0.01
	av	0.004	0.003	0.006	0.002
$\mu_h + \mu_e$	max	0.12	0.12	0.17	0.18
	av	0.06	0.04	0.08	0.04
$\mu_{PR\text{-}TRMC}$		0.15	0.13	0.13	0.12

[a] Both maximal (in 16 columns) and average (over the columns) values are given for electron, hole, total, and measured by PR-TRMC mobilities. ortho = orthorhombic, hexa = hexagonal lattice. Mobilities at 500 K are very small and not shown here, which is due to a significant structural disorder at this temperature.

Already, from the estimates of the internal reorganization energy and the transfer integral dependence on the lateral angle between the neighbors, one can conclude that for a 45° helical configuration the mobilities in the columnar phase should be higher for holes than for electrons, since the transfer integral for such a rotational angle is higher for the positive charge carriers than for the negative ones. To quantify this conclusion, we used the master equation approach to calculate the mobilities for both holes and electrons, with the rates obtained by the Marcus theory. The results are summarized in Table 2.

(53) Warman, J.; de Haas, M.; Dicker, G.; Grozema, F.; Piris, J.; Debije, M. *Chem. Mater.* **2004**, *16* (23), 4600–4609.
(54) van de Craats, A. M.; Siebbeles, L. D. A.; Bleyl, I.; Haarer, D.; Berlin, Y. A.; Zharikov, A. A.; Warman, J. M. *J. Phys. Chem. B* **1998**, *102*, 9625–9634.
(55) Senthilkumar, K.; Grozema, F.; Bickelhaupt, F.; Siebbeles, L. *J. Chem. Phys.* **2003**, *119*, 9809–9817.
(56) Freed, K. F.; Jortner, J. *J. Chem. Phys.* **1970**, *52* (12), 6272–6291.
(57) Frisch, M. J.; et al. *Gaussian 03, Revision C.02*; Gaussian, Inc.: Wallingford, CT, 2004.
(58) Kirkpatrick, J. *Int. J. Quantum Chem.* **2007**, *108*, 51–56.

For each type of charge carrier two values are given, the highest mobility in a particular column (averaged over time) and the average over all columns and time. The difference between the two values is due to the presence of defects in the columns (i.e., a misalignment of one molecule in the stack), which results in a low transfer integral and consequently low mobility. Dynamics of creation or annihilation of such defects is much slower to probe using MD simulations. Note that Marcus theory tends to slightly overestimate the value of the mobility measured by the PR-TRMC technique. For PDI-$C_{8,7}$, however, only the maximal among all the 16 columns value of the mobility is comparable to the experimentally measured one. This implies that the length of a column composed of 60 molecules exceeds the distances sampled by the PR-TRMC technique (which normally probes only 10−20 molecules). As a result, PR-TRMC is relatively insensitive to occasional stacking defects, while they are accounted for in simulations.

It is very illustrative to see how the distributions of the transfer integral J (and correspondingly the rate) change as a function of temperature. These are shown in Figure 5 for holes. The distributions for electrons have very similar functional dependence, but the amplitude is only about 10% smaller. This is an interesting result: though for the ideal helical distribution with 45° twist the transfer integral for holes is much higher than for electrons, disorder in molecular orientations leads to averaging out of the distributions of transfer integrals. The actual difference in the rates (and hence the mobilities) stems from different reorganization energies for holes and electrons.

The sum of the electron and hole mobilities can be directly compared to the mobility measured by the PR-TRMC technique. As one can see from the Table 2, the agreement is good, especially for the highest mobilities. The factor of 2 is within the error bars of experiment and assumptions of Marcus theory for charge transport. The underestimation might also be due to the presence of defects, which do not heal on the time scales reachable by MD simulations. Neither the experimental nor the simulated values depend significantly on the temperature, leading to the conclusion that no major change in the columnar structure happens in the considered temperature range.

V. Conclusions

An important message of this work is that none of the experimental or theoretical methods used here can alone identify the molecular packing of a partially disordered molecular crystal, because of either limitations on reachable time- and length-scales (molecular dynamics), assumptions about a particular supramolecular arrangement in the interpretation of the data (WAXS), or limited structural information due to DQ filtering and dynamic averaging (NMR). When combined, however, these methods do provide a very powerful tool for studies of partially ordered molecular materials.

We can also conclude that none of the experimental methods alone provides detailed enough knowledge of the morphology to predict the charge carrier dynamics in the system. The latter is extremely sensitive to the positional and orientational molecular distribution functions, not only the averaged intermolecular distances and orientations. On the other side, it would be very difficult to perform MD simulations without the guiding hand of WAXS.

Using a combination of experimental techniques and simulation approaches, we have investigated the supermolecular packing of PDI-$C_{8,7}$ molecules. A helical motif with about 45° twist between the neighboring intracolumnar molecules is found to convincingly explain most of the experimental observations. The best fit of the WAXS data is obtained by using a monoclinic unit cell with $a = 21.9$ Å, $b = 17.9$ Å, $c = 3.55$ Å, and $\gamma = 97.8°$.

The azimuthal dependence of the transfer integral shows that the best mobility for both holes and electrons is achieved for a face-to-face supramolecular arrangement. The next maxima are located at ca. 66° azimuthal twist for electrons and around 50° twist for holes.

Although PDI-$C_{8,7}$ is usually perceived as an electron transporter, our simulations predicts that PDI-$C_{8,7}$ is a better hole than electron conductor. The reason for this is different reorganization energies, which result in an order of magnitude smaller hopping rates for electrons than for holes. The difference in transfer integrals (electronic couplings) for electrons and holes accounts only for a 10% discrepancy due to smearing out by the local disorder. This observation is in agreement with time-of-flight measurements of mobility on similar perylene diimide compounds, which indeed find very similar values of mobility for electrons and holes.[59] It is probable therefore that the reason PDI-$C_{8,7}$ does not make a good hole transport is its deep ionization potential.

Acknowledgment. This work was partially supported by DFG via IRTG program between Germany and Korea and DFG grant AN 680/1-1. J.K. acknowledges the support of EPSRC. V.M. acknowledges Alexander von Humboldt foundation. D.W.B. and J.D. acknowledge the Norwegian Research Council for financial support. Daniel Sebastiani, Michael Ryan Hansen, and Robert Graf are acknowledged for fruitful discussions. We thank Karen Johnston, Kurt Kremer, and Thorsten Vehoff for critical reading of the manuscript.

Supporting Information Available: Additional information about experimental and computational details as well as the complete ref 57. This material is available free of charge via the Internet at http://pubs.acs.org.

JA900963V

(59) Kim, J.; Chung, I.; Kim, Y.; Yu, J. *Chem. Phys. Lett.* **2004**, *398* (4−6), 367–371.